Density Functional Theory Studies of the Structure Sensitivity of Ethanol Oxidation on Palladium Surfaces

E. D. Wang, J. B. Xu, and T. S. Zhao*

Department of Mechanical Engineering, The Hong Kong University of Science and Technology, Clear Water Bay, Kowloon, Hong Kong SAR, China

Received: February 09, 2010; Revised Manuscript Received: May 04, 2010

In this work, the adsorption behaviors and oxidation mechanisms of ethanol on palladium surfaces, including the closed-packed Pd(111), the stepped Pd(110), and the open Pd(100), are investigated using density functional theory (DFT). By exploring the electronic properties of different single palladium surfaces, the adsorption behaviors, and the first step dehydrogenation of ethanol, it is found that Pd(100) is the best surface for the dissociation of ethanol molecules. The reaction network of ethanol oxidation on the Pd(100) surface is then investigated to illustrate the complete reaction paths. The results demonstrate for the first time that the activity and selectivity of ethanol oxidation on palladium are highly structure-sensitive. In addition, the effect of OH species on the reaction paths is also studied. The results show that the adsorbed OH species assists in lowering the barrier energy of the CH_2CHOH species oxidizing to the acetic acid species.

1. Introduction

Ethanol is an ideal choice as a fuel for direct oxidation fuel cells due to its high theoretical mass energy density (8030 Wh kg^{-1}), nontoxicity, and its availability from biomass resources.[1,2] The study of ethanol electrooxidation has, therefore, attracted significant attention over past several decades. However, as ethanol has a more complicated molecular structure than methanol and hydrogen have, the kinetics of ethanol electrooxidation is slow, even with a Pt-based catalyst, which is the best catalyst known to date. As a result, the performance of direct ethanol fuel cells (DEFCs) is generally poor.[3,4] The development of electrocatalysts for efficient ethanol oxidation is, therefore, crucial and, also, a big challenge. Encouragingly, recent studies have shown that palladium can act as a good catalyst in alkaline media with a high electrocatalytic activity and a relatively stable behavior for ethanol electrooxidation in DEFCs.[5−7] Notable efforts have been carried out to design palladium-based catalysts and to investigate the electrocatalytic properties of ethanol oxidation. In this regard, the past efforts have mainly focused on catalyst preparation method innovations,[8,9] supports choices,[10] combination with other metals or metal oxides,[11−13] etc. Relatively, the study of the structure sensitivity of ethanol electrooxidation on palladium is scarce. An important question that arises is whether the electrocatalytic activity of atoms located on different Pd crystal facets is different.

Actually, the structure−activity relationship has long been an important issue in heterogeneous catalysis.[14−16] It has been shown that the electrocatalytic activity and selectivity of a catalyst can be greatly enhanced by the use of nanocrystals enclosed by specific crystal facets that are intrinsically more active for a particular reaction.[17−19] As the ethanol electrooxidation reaction on palladium is a typically multistep and multiselectivity heterogeneous catalytic process with a complex network of elementary steps, the structure of palladium catalysts can greatly affect the ethanol oxidation reaction due to the various atomistic properties and adsorption behaviors on different palladium crystal facets. Therefore, the investigation of the effects of different palladium crystal facets on the electrooxidation of ethanol is a crucial task. On the other hand, as mentioned above, ethanol electrooxidation is a multistep reaction. This reaction can be competitively conducted by several possible reaction pathways and yield corresponding intermediates. Some of them might poison the catalyst, resulting in the degradation of the catalyst. The improvement of the electrocatalytic activity of palladium toward ethanol electrooxidation requires the reduction of the effect of those intermediates as far as possible. Therefore, the exploration of the possible intermediate products and the main products is necessary and helpful to the design of efficient catalysts, and thus, to map a complete reaction network for ethanol oxidation on palladium surfaces is another important task. However, unlike Pt-based catalysts,[20−23] the studies of the structure sensitivity and the reaction mechanisms of ethanol electrooxidation on palladium surfaces are relatively scarce.[24]

In this work, we report on a density functional theory (DFT) study on the reaction mechanisms for electrooxidation of ethanol on palladium surfaces, aiming to gain a better understanding of two important issues: (i) surface structure effects on the activity and (ii) reaction mechanism of ethanol electrooxidation on Pd single crystals. Three most common types of palladium surfaces, namely, the closed-packed (111) surface, the monatomic steps represented by Pd(110), and the open (100) surface, are considered. First, the electronic properties of different palladium surfaces and the interactions between an ethanol molecule and palladium surfaces were investigated to determine the most active surface. The most active surface was then further confirmed by calculating the reaction barriers of the first step dehydrogenation of an ethanol molecule on different palladium surfaces systematically. Finally, complete electrooxidation pathways of ethanol on the most active palladium surface were explored to demonstrate the activity and the selectivity. In addition, we paid attention to the role of the hydroxyl groups presented on the most sensitive palladium surface in the real catalytic reaction processes. This work will contribute to a fundamental understanding of the structural, energetic, and

* To whom correspondence should be addressed. Tel: 00852 2358-8647. Fax: 00852 2358-1543. E-mail: metzhao@ust.hk.

10.1021/jp101244t
Published on Web 05/20/2010

catalytic properties of palladium catalysts for ethanol electrooxidation and will be helpful to promoting the design and development of novel anode catalysts for DEFCs.

2. Computational Details

All the calculations in this work were performed using ab initio DFT together with the generalized gradient approximation (GGA) of Perdew, Burke, and Ernzerhof (PBE) for the exchange-correlation potential and the projector augmented wave method (PAW) for ion−electron interactions.[25−29] Periodic slabs based on the (3 × 3) surface unit cell were used as a good compromise between the desire to reduce defect−defect interaction and computational limitations.

Among the different surfaces of palladium crystals, the three most common types of palladium surfaces, namely, the closed-packed (111) surface, the monatomic steps as represented by Pd(110), and the open (100) surface, were considered. All the metal surfaces were modeled with four-layer slabs, with the top two layers being relaxed. The slabs were separated from their periodic images normal to the surface by a vacuum gap (15 Å) that was large enough to eliminate slab−slab interactions. A 4 ×4 × 1 Monkhorst−Pack *k*-point mesh was utilized for all geometry optimization calculations. Optimized geometries were obtained without symmetry constraints, using an energy convergence tolerance of 1×10^{-4} eV and a gradient convergence of 5×10^{-2} eV Å^{-1}. Gaussian smearing with a width of 0.1 eV was employed for calculating partial occupancies. All the calculations on Pd(100), Pd(110), and Pd(111) were fully spin-polarized to allow full relaxation with respect to spin to occur.

Prior to calculating the electrooxidation of ethanol, we examined the interaction between ethanol molecules and Pd single-crystal surfaces to determine the adsorption configurations of ethanol−Pd systems with the lowest energy. Two possible adsorption manners are considered, including the ethanol molecule perpendicular and parallel to the palladium surfaces. The transition states for the electrooxidation reaction of ethanol on Pd(100), Pd(110), and Pd(111) surfaces were then investigated using DFT combined with a new formulation of the linear (LST) and quadratic synchronous transit (QST) methods.[30] Using these two energy points, the LST optimization carries out a series of single-point energy calculations for structures that are linearly interpolated between reactant and product. Once the maximum energy structure along the LST path is found, a conjugate gradient (CG) optimization of this structure is performed.[31] After the residual forces fall below a specified tolerance, the calculation is considered to be converged and can be further analyzed. Otherwise, a new maximum is searched along the QST path connecting reactant, product, and current best transition-state structure. A new CG optimization cycle is then initiated until convergence is achieved. Once the calculations have been converged, the vibrational spectrum of the predicted transition-state structure should have exactly one mode with a negative vibrational frequency ν_{TS}. Because the transition state is characterized by a saddle point on the energy hypersurface, the eigenmode corresponding to ν_{TS} illustrates the directions in which the system would evolve away from this saddle point, following the minimum energy reaction pathway. In this work, Materials Studio 4.4 was used to perform calculations.

3. Results and Discussion

3.1. Atomistic Details of Different Surface Slabs. To demonstrate the structure sensitivity of ethanol oxidation on palladium, it is essential to view the surface properties of the catalyst, which play an important role in the selective catalytic reaction. Here, the electronic states of palladium were investigated by examining the band structures of Pd(100), Pd(110), and Pd(111) with the Fermi level set at 0.0 eV. From Figure 1, one can observe that all the surfaces Pd(100), Pd(110), and Pd(111) appear to be metallic with the energy bands crossing the Fermi level. The Fermi energy of Pd(100) crosses the highest occupied bands, and the electronic band for Pd(100) around the Fermi level appears to be continuous, which will favor the electronic interaction occurring on the surface. This energetic order should allow electrons to easily transfer from the active layer surface to the electron acceptor materials. In the case of Pd(110) and Pd(111), it can be clearly observed that fewer energy bands cross the Fermi level, and the electronic bands present to be sparse near the Fermi level, resulting in a weak electronic behavior and activity.

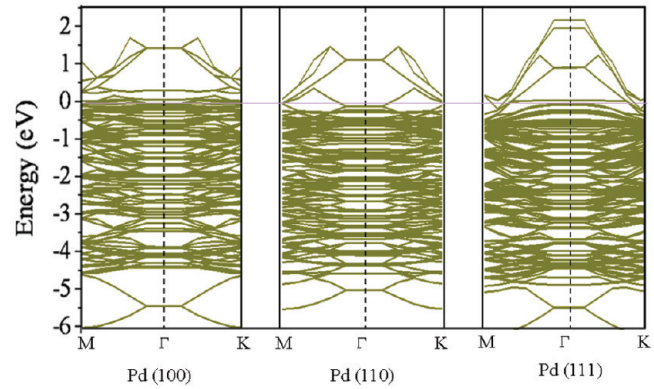

Figure 1. Electronic energy band structures of Pd(100), Pd(110), and Pd(111) surfaces.

To further investigate the electronic properties of palladium, the Mulliken overlap populations, charges, and electronic orbital populations of different Pd atoms on the most outer atomic layer and the second atomic layer for Pd(100), Pd(110), and Pd(111) were calculated and are listed in Table 1. From the calculation results, we can observe that the surface Pd−Pd bonds are stronger than Pd−Pd bonds between the first and the second layer for Pd(100) and Pd(111), as indicated by the overlap population values in Table 1. Especially, the overlap population of the surface Pd−Pd bonds for Pd(100) is the highest among the three Pd surfaces, leading to a strong interatomic interaction. In addition, the surface atoms possess a higher electron density than those in the second layer. This electron density distribution between the surface atoms and the atoms in the second layer for Pd(100) and Pd(111) offers the benefit to electron transfer from the palladium surfaces to the reactant, as it acts as electron donor in the process of surface interactions. However, according to the overlap population and charge population value calculated for Pd(110), it is found that the surface Pd−Pd bond is equal to the Pd−Pd bond between the first and the second atomic layer, and more charge density can be observed in the second layer rather than the first layer. Less Mulliken charge population in the first layer of Pd(110) shows less metallic properties during electronic interaction. The above results indicate that surface atoms of Pd(100) allow more interatomic interaction compared with those of Pd(110) and Pd(111) because of forceful electron coupling along the surface plane. Thus, the atoms in the surface layer of Pd(100) are more sensitive in the electrocatalytic reaction of ethanol. The electronic and catalytic properties of the palladium surfaces will be further investigated by analyzing the interactions between the ethanol molecule and these surfaces.

3.2. Interaction between Ethanol and Pd Surfaces. The adsorption of ethanol on the catalyst surface is a crucial step in

TABLE 1: Overlap Populations, Charges, and Electronic Orbital Populations of Pd Atoms for Pd(100), Pd(110), and Pd(111) Surfaces[a]

	overlap population				orbital occupation		
system	surface	1st−2nd layer	atom	charge	s	p	d
Pd(100)	0.19	0.06	Pd^{first}	−0.09	0.65	0.14	9.30
			Pd^{second}	0.19	0.57	0.01	9.23
Pd(110)	0.11	0.11	Pd^{first}	0.06	0.60	0.03	9.32
			Pd^{second}	−0.11	0.70	0.15	9.26
Pd(111)	0.12	0.04	Pd^{first}	−0.13	0.68	0.16	9.28
			Pd^{second}	0.26	0.55	−0.02	9.20

[a] Two types of Pd−Pd bonds are considered: both Pd atoms on the surface and one Pd atom on the surface and the other on the second layer.

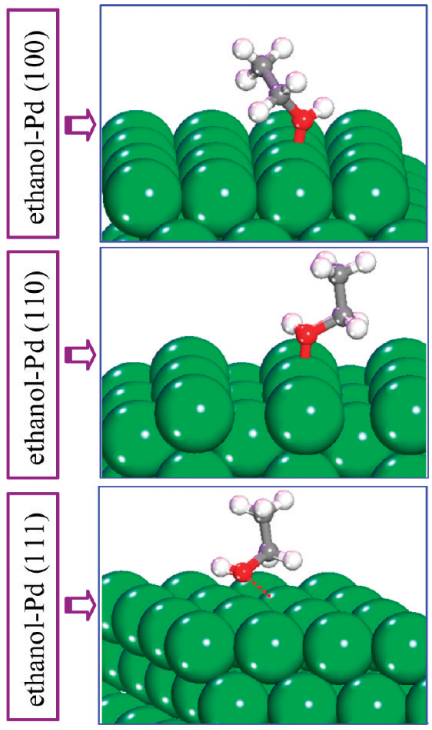

Figure 2. Optimized geometries of an ethanol molecule interacting with Pd (100), Pd (110), and Pd (111) surfaces.

TABLE 2: Binding Energies (E_B) Calculated for the Ethanol−Palladium Configurations Shown in Figure 2 and Minimum Distances (d_{min}) between the Atom in the Ethanol and the Palladium Surface Atoms

configurations	E_B (eV)	d_{min} (Å)
ethanol−Pd (100)	−2.43	2.26
ethanol−Pd (110)	−2.40	2.27
ethanol−Pd (111)	−2.06	2.38

the electrooxidation of ethanol. The interactions between the ethanol molecule and different palladium surfaces were examined. Figure 2 shows the ethanol adsorption configurations on Pd(100), Pd(110), and Pd(111). It is found that the ethanol molecule prefers to adsorb on the palladium atom in a perpendicular way with the oxygen atom close to the surface. The overlap population between the oxygen and the palladium atom is 0.23, 0.18, and 0.17 for the ethanol−Pd(100), ethanol−Pd(110), and ethanol−Pd(111) systems, respectively.

Table 2 lists the binding energies calculated for the ethanol−Pd configurations shown in Figure 2 and minimum distances (d_{min}) between the atoms in the ethanol molecule and the palladium surface atoms. The binding energies for the systems under consideration were obtained from

$$E_B = E(\text{ethanol} + S) - E(\text{ethanol}) - E(S) \quad (1)$$

where E(ethanol + S) is the energy of the final optimized adsorption configuration, E(ethanol) is the energy of the ethanol molecule, and E(S) is the energy of Pd (100), Pd (110), or Pd (111). With this definition, a negative E_B value corresponded to a stable adsorption on the surface.

It can be seen from Table 2 that the bonding energies are −2.43, −2.40, and −2.06 eV for ethanol−Pd(100), ethanol−Pd(110), and ethanol−Pd(111), respectively. The results indicate that the interaction between the ethanol and Pd(100) is stronger than those of Pd(110) and Pd(111). The ethanol−Pd(100) also exhibits the smallest distance among the three structures. The strong interaction between ethanol and the Pd surface offers a benefit to the further catalytic reaction.

Figure 3 presents the partial electronic density of states (PDOS) for the surface palladium atom (black curves), the oxygen atom of the ethanol (blue curves), and the surface palladium atom bonding to the oxygen atom (red curves). From Figure 3a,b, it can be observed that a split occurs for the hybrid orbital of 4p, 5s, and 4d orbitals of the palladium atom, which bonds to the oxygen atom of the adsorbed ethanol molecule. The new pair of molecular orbitals referring to the two new peaks appearing in the range of −7.7 to −6.8 eV and −6.0 to −5.2 eV were split by the interaction energy between the ethanol molecule and the palladium surface; −7.7 to −6.8 eV corresponds to the bonding orbital and −6.0 to −5.2 eV corresponds to the antibonding orbital. The −4.0 to 0.0 eV below the Fermi level (0.0 eV) is related to the electron repopulation in the valence shell of palladium atoms. These results prove that a strong interaction exists between the ethanol molecule and the open Pd(100) surface, which is also verified by the binding energies in Table 2. The electronic interaction between the ethanol molecule and the Pd(110) surface is localized in two ranges, −7.7 to −5.0 eV and −5.0 to 0.0 eV, as shown in Figure 3b. The level around −7.7 to −4.8 eV exhibits a relative slight split of the hybridized orbital of the valence shell for palladium atoms, which presents the bonding orbital to the O−Pd on Pd(110) at −7.7 to −6.5 eV and the antibonding orbital at −5.8 to −4.8 eV. Electronic interaction happens between the ethanol molecule and the Pd(110) surface with electron repopulation in the valence shell of palladium atoms at −5.0 to 0.0 eV. In Figure 3c, an obvious peak can be seen in the PDOS of Pd($4s^2 4p^6 4d^{10}$) near the oxygen in the range of −7.5 to −6.5 eV for ethanol−Pd(111), indicating that a strong electronic interaction occurs to the hybridized orbital in the valence shell of palladium atoms close to the ethanol molecule. However, although a new peak appeared at around −7.0 eV, no obvious split of the hybridized orbital in the valence shell of palladium atoms can be observed, which corresponds to the relative lower interaction energy between the ethanol molecule and the

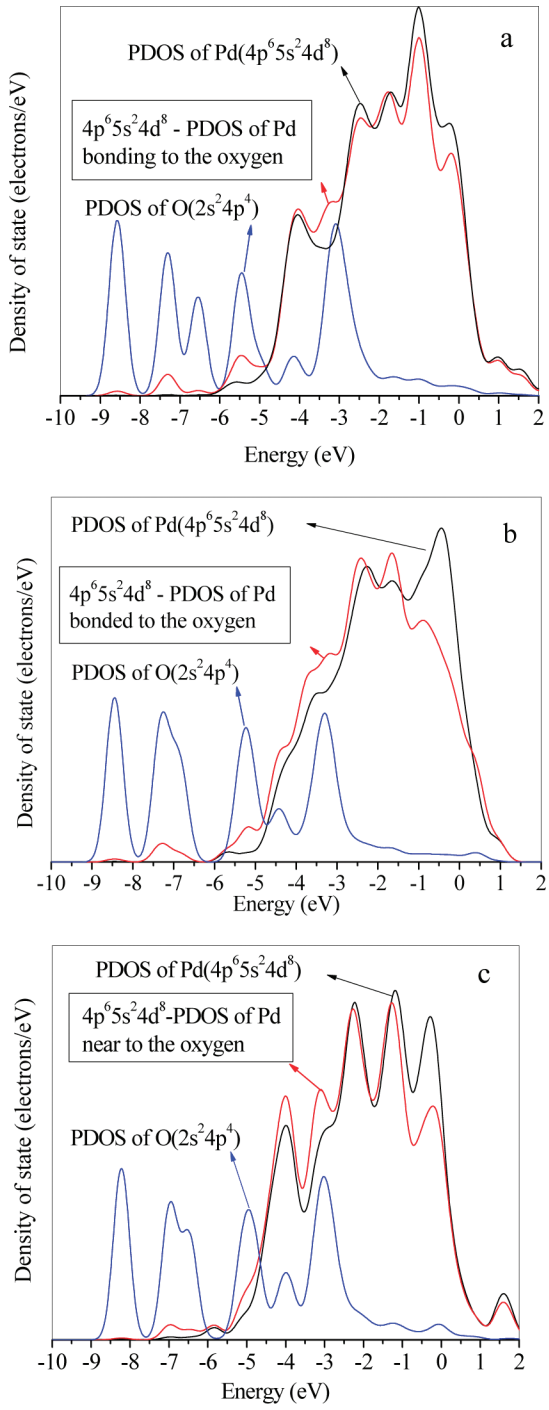

Figure 3. Partial electronic densities of states for three interaction systems calculated for the corresponding configurations shown in Figure 2: (a) ethanol−Pd(100), (b) ethanol−Pd(110), and (c) ethanol−Pd(111).

palladium surface. Generally, the oxygen atom has the lower energy orbitals because electrons are lower in energy where they are better stabilized, as shown in Figure 3. However, due to the strong interaction between the ethanol molecule and Pd(100), the s−p hybrid orbital of the oxygen atom shows a split in the level of −8.0 to −6.0 eV. The split of the s−p hybrid orbital of the oxygen atom will lead to closer in energy to the hybrid orbital of 4p, 5s, and 4d orbitals of the palladium atom, especially the slight peak for palladium at around −6.5 eV, which favors the interaction between the ethanol molecule and Pd(100). Therefore, conbining the result of binding energy and the PDOS analysis, we found that the interaction of ethanol to Pd(111) is relatively more slight than those to Pd(100) and Pd(110).

The analysis of geometric structures, binding energies, and the electronic properties shows that the interaction of the ethanol molecule with the open Pd(100) surface is stronger than those with the stepped Pd(110) and the close-packed Pd(111).

3.3. Dehydrogenation of Ethanol on Pd Surfaces. On the basis of the above ethanol−Pd configurations, the electrocatalytic activities of palladium surfaces to ethanol oxidation were investigated by detecting each "likely" bond cleavage of the ethanol molecule with breaking its CH and OH bonds on Pd(100), Pd(110), and Pd(111). By "likely", we mean that the reaction route must have relatively low reaction barriers, typically below 0.75 eV (a magnitude regarded as a surmountable barrier for reactions occurring at room temperatures).

Figure 4 shows the calculated potential energy profiles for the dehydrogenation of the ethanol by breaking its CH and OH bonds on the Pd(100) surface. The reactions initiate from the optimized geometries of the ethanol−Pd(100) system. Three reaction channels, path 1 (hydroxyl break), path 2 (α-H release, α-H = $CH_3C\boldsymbol{H}_2OH$), and path 3 (β-H release, β-H = $C\boldsymbol{H}_3CH_2OH$), are energetically close.

In path 1, the ethanol molecule dissociates into CH_3CH_2O and H, which is found to be exothermic by 0.36 eV together with a barrier energy of 0.70 eV. The electronic properties of the system at the critical points, that is, the initial state, transition state, and final state, show that the ethanol molecule is decomposed into CH_3CH_2O and H with the electron transfer from the atoms of Pd(100) to the adsorbed ethanol molecule. The total charge transfer (Q_t) from the surface slab to the adsorbed ethanol molecule, denoting to be positive, is 0.79 e^- at the transition state. With the repopulation of electron density between the absorbent and the absorbate, Q_t is 0.64 e^- at the final state, in which the ethyoxyl group (CH_3CH_2O) is bonded to the Pd site and hydrogen is transferred to the bridge site of two palladium atoms of the surface layer of Pd(100).

In an analogous way, ethanol dissociation along path 2 on Pd(100) associates to a C−H breaking process and the formation of CH_3CHOH and H. In TS_2, we obtained a qualitatively similar one-step reaction mechanism for the three channels of the ethanol−Pd(100) systems from the viewpoint of electron transfer. The atomic charge distribution of the system at the critical points, that is, the initial state, transition state, and final state, shows partial electron transfer from the atoms of Pd(100) to the ethanol molecule. As CH_3CH_2OH dissociates on the open Pd(100) surface, the s and d orbital populations of the surface palladium atom decrease, resulting in a charge reduction on the palladium surface. With this reduction, the electronic interaction occurs between the absorbent and the absorbate, and a break happens to the C−H at the α-position. Q_t from the surface slab to the adsorbed ethanol molecule is 0.60 e^- at the transition state. At the final state, the atoms of CH_3CHOH and the H gain a negative charge of 0.42 e^-; as a result, there is a transfer of electron density from the atoms of the Pd(100) surface to the CH_3CHOH and the H. These results further verify the strong electronic interaction between Pd(100) and the ethanol molecule, leading to the dissociation of ethanol on Pd(100). However, although the effect of electron density repopulation between the absorbent and the absorbate in path 2 is weaker than that in the path 1, the dissociation of the ethanol molecule can be more accessible. That is because the total energy barrier for this process is 0.29 eV, which is a low energy barrier for α-dehy-

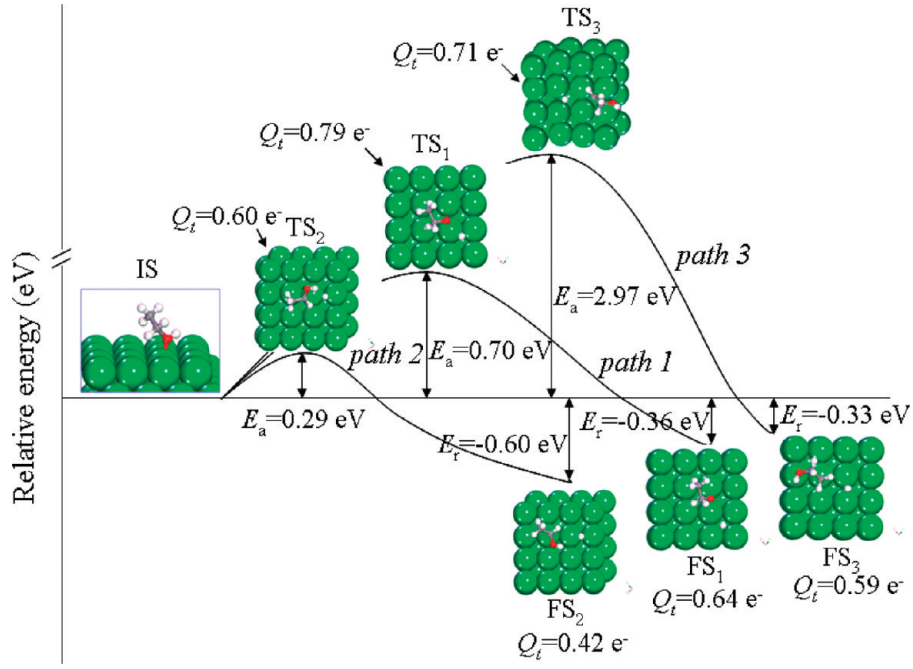

Figure 4. Calculated potential energy profiles given in eV for the decomposition of ethanol on Pd(100). Distances are given in units of angstroms. Total charge transfer, (Q_t), is denoted to be positive when charges transfer from the atoms of Pd(100) to the adsorbate. The IS, TS, and FS denote the initial state, transition state, and final state, respectively.

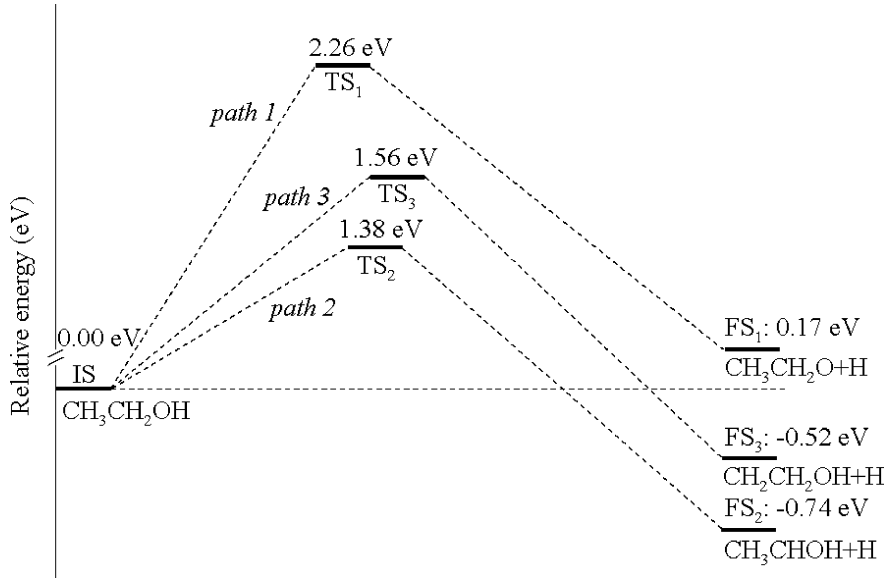

Figure 5. Potential energy diagram for the dehydrogenation of ethanol on Pd(110).

drogenation of the ethanol molecule. This process is found to be exothermic by 0.60 eV.

Regarding path 3, the energy barrier is 2.97 eV, which is far higher than those in path 1 and path 2. The corresponding transition states TS_3 involve the β-dehydrogenation and the formation of CH_2CH_2OH and H. If there is enough active energy, the ethanol dehydrogenation reaction on Pd(100) through the path 3 channel can be exothermic by 0.33 eV. However, with such a high barrier energy (2.97 eV), the ethanol molecule can hardly dissociate into CH_2CH_2OH and H on Pd(100). It is found that the ethanol dehydrogenation reactions on Pd(100) through path 1 and path 2 can be easily accessible with a relatively low barrier energy.

Figure 5 shows the energy profiles for the dehydrogenation of the ethanol by breaking its OH (path 1), α-CH (path 2), and β-CH (path 3) bonds on Pd(110). The one-step reactions initiate from the optimized geometries of the ethanol−Pd(110) system. The path 1, path 2, and path 3 channels of the reaction are energetically adverse. The barrier energies for the reactions of the path 1, path 2, and path 3 channels are 2.26, 1.38, and 1.56 eV, respectively, indicating that all reaction channels are difficult to access.

The energy profiles for the dehydrogenation of the ethanol molecule by breaking its OH (path 1), α-CH (path 2), and β-CH (path 3) bonds on Pd(111) are presented in Figure 6. The dehydrogenation reaction through path 1 and path 3 on Pd(111) is found to be exothermic by 0.19 and 0.02 eV, respectively. The reaction through path 2 is observed to be endothermic by 0.74 eV. The barrier energy for path 1 is very high (2.27 eV). However, the barrier energy for path 2 and path 3 is 1.19 and 1.01 eV, which is far lower than that of path 1 (2.27 eV). The results indicate that α-dehydrogenation and β-dehydrogenation

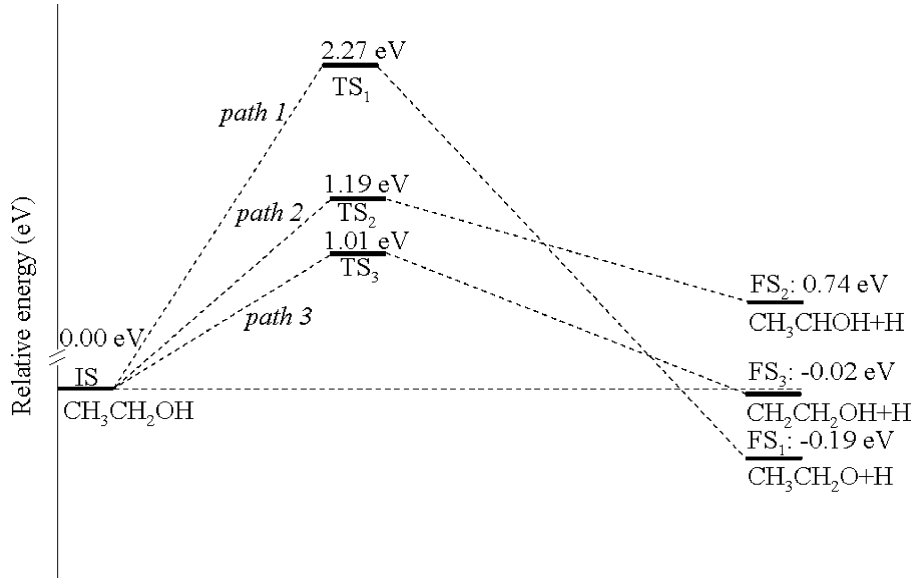

Figure 6. Potential energy diagram for the dehydrogenation of ethanol on Pd(111).

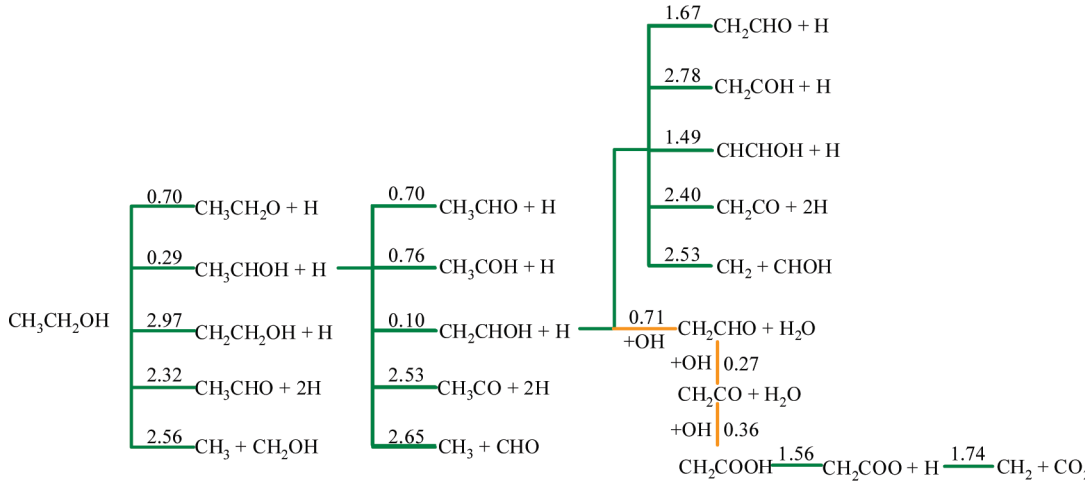

Figure 7. Calculated reaction network through the most possible paths with the lowest reaction barriers (units, eV) for ethanol oxidation on Pd(100). H atoms and H_2O molecules produced are omitted in the following step for clarity. The data in parentheses are the energy barriers after the zero-point-energy correction.

are more accessible than the break of OH on Pd(111). In comparison to the partial activation barriers at the transition states TS_1, TS_2, and TS_3 in Figure 6, the migration of the H atom from the ethanol to the palladium atom of the Pd(111) favors the path 3 channel. According to the Mulliken charge population analysis, the atomic charge distribution of the system at the critical points of the reactions shows partial electron transfer from the Pd(111) atom to the absorbate, leading to the dehydrogenation of the ethanol. Although the barrier (1.01 eV) of path 3 is lower than those of the other two paths, it is still high for a reaction to take place at room temperature. This might be the explanation of the nonactivity of Pd-based catalysts for electrooxidation of ethanol in acid media, due to that the Pd(111) is the dominant surface in common Pd catalysts.[32]

Taking the above results into consideration, we found that Pd(100) is more efficient than Pd(110) and Pd(111) in the electrooxidation of ethanol, according to the calculated barrier energies, which can also be proved by the analysis of the electronic properties of Pd(100), Pd(110), and Pd(111).

3.4. Reaction Network of Ethanol Oxidation on Pd Surfaces. The above results show that ethanol can release hydrogen easily by breaking its CH and OH bonds on Pd(100) but hardly dissociates on Pd(110) and Pd(111). Therefore, we further explore the complete reaction network for ethanol electrooxidation on the active Pd(100) surface. To map out the whole reaction network, a recursive "trial-and-error" approach is taken by the new constrained Broyden minimization technique, in which the high work load is largely eased.[23] In addition, to deduce a complete mechanism of the ethanol oxidation reaction, the participation of oxidative species, such as hydroxyl, is taken into account.

The calculated reaction network of ethanol oxidation on Pd(100) is illustrated in Figure 7. Here, we aim at establishing a relatively complete reaction map along the path with the lowest barrier energy, in particular, with emphasis on the C−C bond cleavage, which is the final reaction to produce CO_2. As a starting point, five different bond-breaking paths for the initial bond cleavage of ethanol are identified. Combined with the dehydrogenation reaction of ethanol discussed above (Figure 4), it is found that C−C bond breaking and the β-dehydrogenation of the ethanol molecule in the first step are most unlikely, with extremely high reaction barriers of 2.56 and 2.97 eV, respectively. The next most unfavorable path is the formation of acetaldehyde (CH_3CHO), with the energy barrier of 2.32 eV.

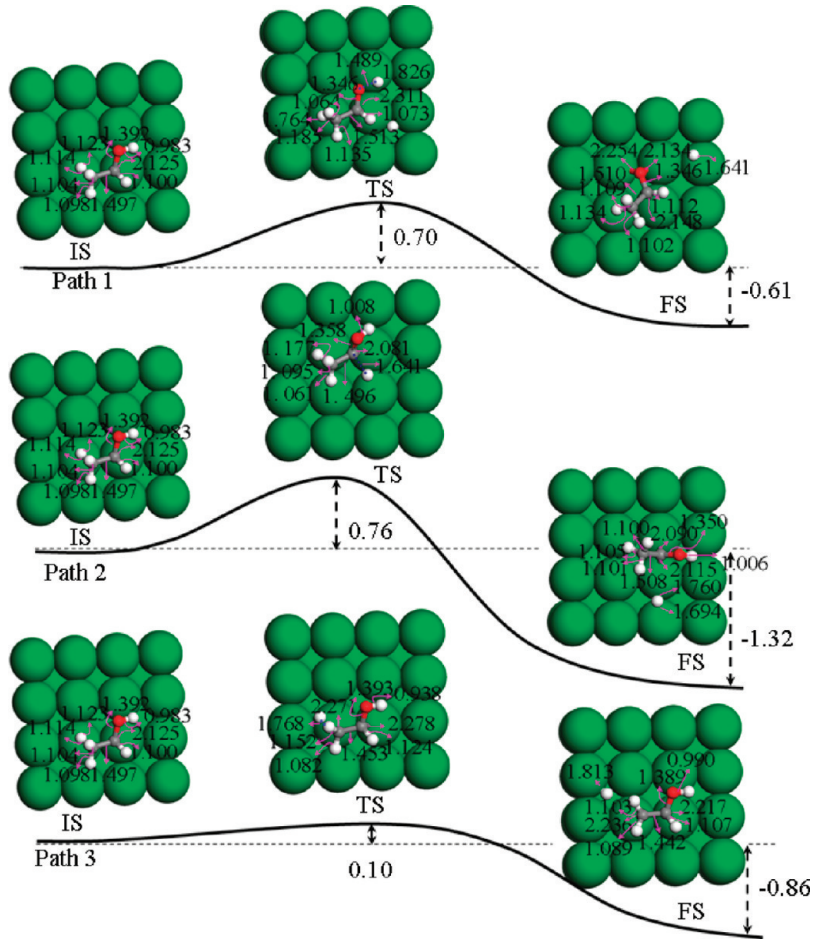

Figure 8. Calculated potential energy profiles given in eV for the adsorbed ethanol species CH_3CHOH dehydrogenation through path 1 (OH scission), path 2 (α-dehydrogenation), and path 3 (β-dehydrogenation). Distances are given in units of angstroms. The IS, TS, and FS denote the initial state, transition state, and final state, respectively.

In the first step of ethanol oxidation, α-dehydrogenation is the pathway with the lowest energy barrier (0.29 eV), which is identified in Figure 4.

In the second step, we analyzed the dehydrogenation reaction paths of CH_3CHOH through path 1 (OH scission to produce acetaldehyde), path 2 (α-dehydrogenation), path 3 (β-dehydrogenation), path 4 (the generation of ketone), and path 5 (C−C bond cleavage). Detailed reaction pathways for path 1, path 2, and path 3 are illustrated in Figure 8. The initial state of this dehydrogenation reaction is the adsorbed CH_3CHOH configuration. The final states are the configurations of OH scission (path 1), α-dehydrogenation (path 2), and β-dehydrogenation (path 3). As shown in Figure 8, the hydrogen atom in the hydroxyl group begins to move away from the CH_3CHOH on Pd(100) through path 1 and then is absorbed to the top of the palladium atom of the surface, resulting in the formation of acetaldehyde. In path 2, the energy barrier of 0.76 eV induces the α-dehydrogenation of CH_3CHOH on Pd(100). With the dissociation of α-H, the final state is the chemical sorption configuration on palladium that shows a bonding between the α-H and two palladium atoms with the distances of about 2.090 and 2.115 Å, respectively. The hydrogen atom is chemisorbed symmetrically to the bridge site of two palladium atoms with the distances of 1.694 and 1.760 Å. The dehydrogenation of CH_3CHOH in path 2 is found to be exothermic by 0.26 eV. Path 3 exhibits an energy barrier of 0.10 eV and indicates that the β-dehydrogenation reaction is an easy reaction. The final state is composed of the hydrogen atom at almost the center of the four-membered ring of palladium atoms and α-C and β-C of CH_2CHOH, which adsorb on the top site of the palladium atom. During the isolation of a hydrogen atom from the initial adsorbed CH_3CHOH state to its final state, the C−C axis showed a rotation to the most stable parallel configuration of the adsorbed state on the Pd(100) surface. In this process, the hydrogen would be brought close enough to the surface through a proximal effect, which may be induced by the bond between H−Pd, resulting in the adjusting of the O−C and C−C at the transition state. From the final states of path 1, path 2, and path 3, it is found that the bond lengths of C−H and O−H in path 3 are shorter than those in path 1 and path 2. These results indicate that path 3 is the favorite channel for the dehydrogenation of CH_3CHOH. The reason can be interpreted with the BEP (Bell−Evans−Polanyi) principle: the more stable the products, the lower the activation barrier. Also, at the initial state, the hydrogen atom of CH_3CHOH bonded to the atoms of Pd(100), which becomes more active due to the electronic interaction with the surface palladium atom. The special electronic structure of the adsorbed CH_3CHOH together with the electronic effect of the Pd(100) surface promotes the dehydrogenation of CH_3CHOH through path 3.

Path 4 and path 5 show that the energy barriers for the formation of ketone and C−C bond cleavage are 2.53 and 2.65 eV, respectively. These high reaction barriers prevent the formation of ketone and C−C bond cleavage. In summary, in the second step, the β-dehydrogenation (path 3) possesses the

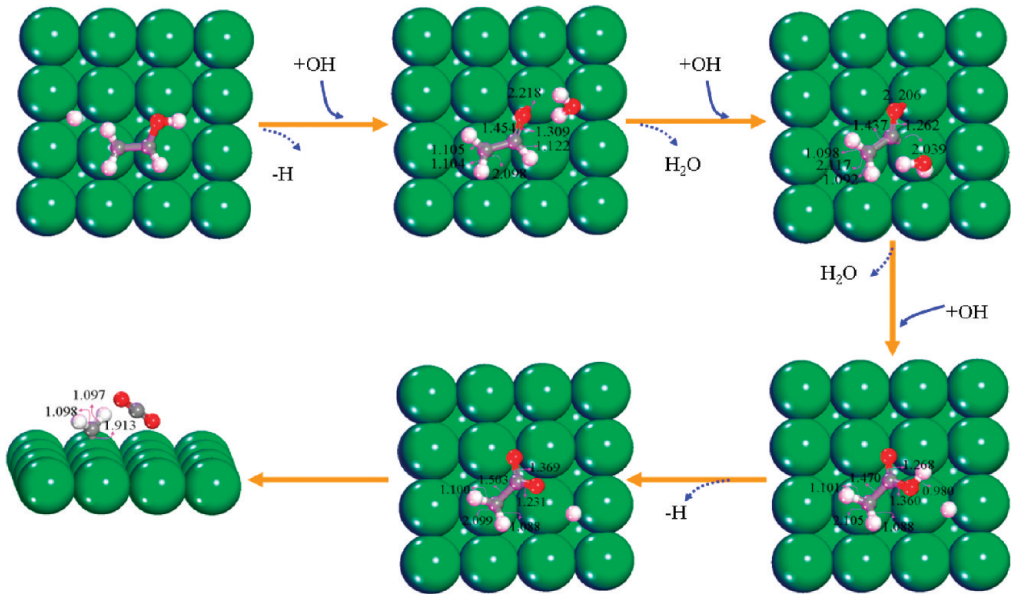

Figure 9. Stable geometric optimized structures of the dissociation of the acetic acid species by the oxidation of OH on Pd(100).

lowest reaction barrier of 0.10 eV among the five paths and is more accessible than the other reaction channels.

According to the calculated energy barriers in Figure 7, further dehydrogenation of CH_2CHOH became rather difficult with all the paths hindering by reaction barriers greater than 1.0 eV. Hence, to the third step, the effect of the hydroxyl group to further oxidize CH_2CHOH on Pd(100) is discussed. Under oxidative conditions, where oxidative species, such as OH, are present (at higher potential, e.g., above 0.5 V[33]), it is found that CH_2CHOH can react with hydroxyl easily with an energy barrier of 0.71 eV to yield CH_2CHO. CH_2CHO is then oxidized to CH_2CO by the help of OH with an energy barrier of 0.27 eV, and CH_2CO further reacts with OH, generating into CH_2COOH immediately with an energy barrier of 0.36 eV. Figure 9 shows the optimized geometric structures for OH attacking CH_2CHOH to obtain CH_2COOH and the breakage of the C−C bond to form CO_2 on Pd(100). The reaction between CH_2CHOH and OH is exothermic with a reaction energy of 2.19 eV (1.48 eV below the entrance barrier), providing the CH_2CHO adduct with a significant amount of excess vibrational energy. In addition, dissociation of the O−H bond in the CH_2CHOH increases the stability of the CH_2CHO adsorbed on Pd(100). At moderate temperatures, the reaction between CH_2CHOH and OH produces stabilized CH_2CHO due to the adduct formation; the subsequent reactions of this stabilized adduct CH_2CHO with OH are important steps in the complete oxidation of ethanol to form CO_2. In the configuration of the adsorbed CH_2CHO on Pd(100), the β-site C−H bond is shorter than the α-site C−H bond; the overlap population for the β-site C−H bond is higher than that of the α-site C−H bond. With the addition of OH, a water molecule is released and then CH_2CHO is further oxidized by OH to produce CH_2CO with a low reaction barrier of 0.27 eV. In this reaction, the α-H is easily attacked by the OH and a water molecule is generated. The distance between the oxygen atom of the adsorbed CH_2CO and the palladium atom of the Pd(100) surface is 2.206 Å, which is slightly shorter than that of the adsorbed CH_2CHO (2.218 Å). In addition, the bond length between the α-C of the adsorbed CH_2CO and the palladium atom of the Pd(100) surface is 2.039 Å. In the CH_2CO−Pd(100) system, α-C, β-C, and the oxygen atom all bond to the palladium atoms of the surface, leading to the stability of the CH_2CO−Pd(100) structure. Hence, the oxidation to CH_2CO on Pd(100) is further investigated. The α-C of CH_2CO appears to be positive in Mulliken charge on Pd(100) and reacts with OH as a barrier of 0.36 eV to generate CH_2COOH. As a result, CH_2COOH adsorbs on Pd(100) for only the β-C bonding to palladium atom with the distance of 2.105 Å. This reaction provides a significant contribution to the further oxidation of ethanol.

To this end, we studied the dissociation of acetic acid species on the Pd(100) surface. The most likely path for the dissociation of acetic acid species is the breakage of the hydroxyl. The release of H from the hydroxyl in this step is found to proceed with a barrier of 1.56 eV. It is then expected that the CH_2COO dissociates into CH_2 and CO_2 with the barrier energy of 1.74 eV. Here, CO_2 is released freely and the CH_2 is adsorbed to the top of palladium with a distance of 1.913 Å, as depicted in Figure 9.

The above results show that the selectivity of ethanol oxidation starts from the ethanol to the adsorbed ethanol species CH_2CHOH with the α-C and β-C bond to the palladium atoms on Pd(100) in the reaction network. The adsorbed ethanol species CH_2CHOH is then oxidized by the help of OH, forming the acetic acid species. In the latter, with the breakage of the hydroxyl bond and the C−C bond in the acetic acid species, a free CO_2 molecule and the adsorbed CH_2 are finally produced with a high energy barrier.

4. Conclusions

We have investigated the electrocatalytic activity and selectivity of palladium to ethanol oxidation using the closed-packed Pd(111), the stepped Pd(110), and the open Pd(100) surfaces. The binding energies of ethanol interacting to Pd(100), Pd(110), and Pd(111) are −2.43, −2.40, and −2.06 eV, respectively. According to the calculated barrier energies of ethanol dehydrogenation on Pd(100), Pd(110), and Pd(111), it is found that the strong interaction between ethanol and the surface of palladium led to the lowest barrier energies for ethanol dehydrogenation on Pd(100). The results demonstrated for the first time that the activity and selectivity of ethanol oxidation on palladium are highly structure-sensitive and proved that Pd(100) is the best surface for the dissociation of an ethanol molecule with a rather low energy barrier. We then further investigate

the subsequent steps of electrooxidation of ethanol on the active Pd(100) surface, where, in the presence of OH, a complete ethanol oxidation reaction is carried out. The investigations in this work will motivate theoretical and experimental studies on the ethanol oxidation reaction and assist in the development of novel anode catalysts in DEFCs.

Acknowledgment. The work described in this paper was supported by a grant from the Research Grants Council of the Hong Kong Special Administrative Region, China (Project No. 623008).

References and Notes

(1) Wang, H. F.; Liu, Z. P. *J. Phys. Chem. C* **2007**, *111*, 12157.
(2) Arico, A. S.; Creti, P.; Antonucci, P. L.; Antonuccci, V. *Electrochem. Solid-State Lett.* **1998**, *1*, 66.
(3) Mann, J.; Yao, N.; Bocarsly, A. B. *Langmuir* **2006**, *22*, 10432.
(4) Tsiakaras, P. E.; Douvartzides, S. L.; Demin, A. K.; Sobyanin, V. A. *Solid State Ionics* **2002**, *152−153*, 721.
(5) Mackiewicz, N.; Surendran, G.; Remita, H.; Keita, B.; Zhang, G.; Nadjo, L.; Hagège, A.; Doris, E.; Mioskowski, C. *J. Am. Chem. Soc.* **2008**, *130*, 8110.
(6) Xu, C. W.; Wang, H.; Shen, P. K.; Jiang, S. P. *Adv. Mater.* **2007**, *19*, 4256.
(7) Shen, P. K.; Xu, C. W. *Electrochem. Commun.* **2006**, *8*, 184.
(8) Shen, Q. M.; Min, Q. H.; Shi, J. J.; Jiang, L. P.; Zhang, J. R.; Hou, W. H.; Zhu, J. J. *J. Phys. Chem. C* **2009**, *113*, 1267.
(9) Xiong, Y. J.; McLellan, J. M.; Chen, J. Y.; Yin, Y. D.; Li, Z. Y.; Xia, Y. N. *J. Am. Chem. Soc.* **2005**, *127*, 17118.
(10) Hu, F. P.; Cui, G. F.; Wei, Z. D.; Shen, P. K. *Electrochem. Commun.* **2008**, *10*, 1303.
(11) Liu, Z. L.; Zhao, B.; Guo, C. L.; Sun, Y. J.; Xu, F. G.; Yang, H. B.; Li, Z. *J. Phys. Chem. C* **2009**, *113*, 16766.
(12) Shen, S. Y.; Zhao, T. S.; Xu, J. B.; Li, Y. S. *J. Power Sources* **2010**, *195*, 1001.
(13) Singh, R. N.; Anindita, A. S. *Carbon* **2009**, *47*, 271.
(14) Goodman, D. W.; Peden, C. H. F. *J. Phys. Chem.* **1986**, *90*, 4839.
(15) Peden, C. H. F.; Goodman, D. W. *J. Phys. Chem.* **1986**, *90*, 1360.
(16) Goodman, D. W. *J. Phys. Chem.* **1996**, *100*, 13090.
(17) Narayanan, R.; El-Sayed, M. A. *Nano Lett.* **2004**, *4*, 1343.
(18) Habas, S. E.; Lee, H.; Radmilovic, V.; Somorjai, G. A.; Yang, P. *Nat. Mater.* **2007**, *6*, 692.
(19) Bratlie, K. M.; Lee, H.; Komvopoulos, K.; Yang, P.; Somorjai, G. A. *Nano Lett.* **2007**, *7*, 3097.
(20) Tarnowski, D. J.; Korzeniewski, C. *J. Phys. Chem. B* **1997**, *101*, 253.
(21) Cao, D.; Lu, G. Q.; Wieckowski, A.; Wasileski, S. A.; Neurock, M. *J. Phys. Chem. B* **2005**, *109*, 11622.
(22) Alcala, R.; Mavrikakis, M.; Dumesic, J. A. *J. Catal.* **2003**, *218*, 178.
(23) Wang, H. F.; Liu, Z. P. *J. Am. Chem. Soc.* **2008**, *130*, 10996.
(24) Liang, Z. X.; Zhao, T. S.; Xu, J. B.; Zhu, L. D. *Electrochim. Acta* **2009**, *54*, 2203.
(25) Perdew, J. P.; Zunger, A. *Phys. Rev. B* **1981**, *23*, 5048.
(26) Perdew, J. P.; Wang, Y. *Phys. Rev. B* **1992**, *45*, 13244.
(27) Kresse, G.; Hafner, J. *Phys. Rev. B* **1993**, *47*, 558.
(28) Kresse, G.; Furthmüller, J. *Phys. Rev. B* **1996**, *54*, 11169.
(29) Kresse, G.; Furthmüller, J. *Comput. Mater. Sci.* **1996**, *6*, 15.
(30) Govind, N.; Petersen, M.; Fitzgerald, G.; Smith, D. K.; Andzelm, J. *Comput. Mater. Sci.* **2003**, *28*, 250.
(31) Sinclair, J. E.; Fletcher, R. *J. Phys. C: Solid State Phys.* **1974**, *7*, 864.
(32) Fang, X.; Shen, P. K. *Acta Phys.-Chim. Sin.* **2009**, *25*, 1933.
(33) Climent, V.; Gomez, R.; Orts, J. M.; Feliu, J. M. *J. Phys. Chem. B* **2006**, *110*, 11344.

JP101244T